Silk Fibroin/Chitosan Blended Microparticles: Preparation, Characterization, and Oil Absorption

Ansaya Thonpho , Suchai Tanisood , Wilaiwan Simchuer , Yodthong Baimark , Prasong Srihanam *

Posted Date: 13 May 2026

doi: 10.20944/preprints202605.0850.v1

Keywords: chitosan; emulsion; particles; oil absorption; silk fibroin

 doi:10.20944/preprints202605.0850.v1

Article

Silk Fibroin/Chitosan Blended Microparticles: Preparation, Characterization, and Oil Absorption

Ansaya Thonpho [1], Suchai Tanisood [1], Wilaiwan Simchuer [2], Yodthong Baimark [1] and Prasong Srihanam [1,*]

[1] Biodegradable Polymers Research Unit, Department of Chemistry and Centre of Excellence for Innovation in Chemistry, Faculty of Science, Mahasarakham University, Mahasarakham 44150, Thailand

[2] Faculty of Science and Technology, Loei Rajabhat University, Mueang District, Loei, 42000, Thailand

* Correspondence: prasong.s@msu.ac.th; Tel.: +66-845119244

Abstract

In this work, we extracted silk fibroin (SF) by a tertiary solvent system ($CaCl_2$:Ethanol:H_2O), and then blended with chitosan (CS) solution to construct microparticles using the water−in−oil−emulsion−diffusion method. The mixture of SF/CS solution aqueous phase; W) was prepared at ratios of 4:0, 3:1, 1:1, 1:3, and 0:4, using ethyl acetate as the oil phase (O). After the microparticles were prepared, their morphology was examined using scanning electron microscopy (SEM). The results indicated that the optimal preparation conditions were a 1% (w/v) aqueous phase with a volume of 1 milliliter, 100 milliliters of oil phase, and a stirring speed of 700 rpm. The average microparticle size was 50−100 micrometers.ATR−FTIR spectra showed unique functional groups of SF and CS, as well as interactions between the two polymers. The results of the thermal property study using a TGA instrument showed that SF microparticles had a higher maximum decomposition temperature ($T_{d,\ max}$) than chitosan, and the blended microparticles' $T_{d,\ max}$ increased with the proportion of SF. Most microparticles exhibited a semi-crystalline polymer structure, with SF microparticles being the most hydrophobic, followed by blended microparticles and CS, respectively. Testing for absorption capacity, the SF microparticles were more effective at absorbing used engine oil than vegetable oil and chloroform, while CS microparticles showed the highest capacity for vegetable oil.The experimental results indicated that all SF/CS blended particles played an efficiency of absorption variable by ratios of SF or CS blended. This suggested that the prepared microparticles might be useful for oil/water separation application.

Keywords: chitosan; emulsion; particles; oil absorption; silk fibroin

1. Introduction

A critical worldwide issue is water pollution. There are many causes for this problem including oil and fuel spillage, industrial discharge of organic solvents, and heavy metal ions which resulted severe environmental and ecological damage [1−3]. It is hardly way to control the pollution for the long-term, and effects on aquatic ecosystems [4,5].

With previous reports, oil spill remediation such as dispersants [6], solidifiers [7], absorbents [8−11], controlled burning [12], mechanical collection [13], and biodegradation [14,15] have been widely used for oil/organic solvent cleanup. Among these stretegies, using absorbents is the most promising practical use [4,16]. In general, oil absorbents properties should be composed of several advantages, including high oil sorption capacity, selective oil/water separation, fast oil sorption, low density, cheap, environmentally friendly and reusability [17,18]. Hydrophobic surfaces with interconnected macroporous structure absorbent materials have been developed and proposed. Different forms of oil absorbent materials have also been reported including sponges [19–21], particles [22,23] and aerogels [24–26]. However, most of oil absorbents are inorganic or non-biodegadable materials such as graphene−based sponges [3], melamine sponges [27], and

 doi:10.20944/preprints202605.0850.v1

polyurethane sponges [28], which can be lead to the pollution [29,30]. Therefore, it is critical to use renewable resources to produce biodegradable and environmentally friendly separation materials for oil-water separation. In recent, natural polymers has become extremely interets according their safety and presence of many hydrophilic groups resulting to create superhydrophilic surfaces [21,31]. This characteristic helps reduce oil contamination during the separation process and considered the most effective materials for oil/water separation [32].

The natural protein-based polymer such as silk and cellulose have been used in various applications and forms. The silk fibers are composed of two types of protein called "silk fibroin (SF)" and "silk sericin (SS)" or glue−like protein [33,34]. Generally, SF consisted of high hydrophobic amino acid residues with lower hydrophilic in nature. This amphiphilicity of SF makes it display promising potential in various applications [35−37]. Pickering emulsions stabilized by SF nanobrush formed from the silk nanofibers induced self-assembly of dissolved SF has been reported [38,39]. Many works have reported that SF serves as a proficient stabilizer for oil−in−water emulsions with [40]. SF−based absorbent have drawn a lot of interest for oil/water separation [41]. The surfaces of silk fiber surface have abundant microscopic textures and pores, resulting a natural sieve of oil or water droplets. Those of functional groups such as amino, carboxyl, and hydroxyl groups, in the silk fiber structure are served as ideal reaction sites for chemical modifications [42,43]. Moreover, silk takes an advantage due to environmental friendliness and sustainable development for application in oil−contaminated wastewater or oil spills. In addtion, silk fibers combined other materials in various forms showed increasingly efficiency for oil/water separation [41,44,45].

Chitosan (CS), a natural cationic polysaccharide consisting of repeating units of glucose connected by β-1,4−glycosidic linkages. It is derived from chitin that can be found in the exoskeleton of crustaceans via deacetylation reaction [46]. Among biopolymers, it is an abundant, low−cost and has fascinating qualities including sustainable materials [47,48]. The chemical structure of CS existence of amino and hydroxyl groups, that provide unique characteristics. The amino groups are widely known as positively charged which attached with negatively groups of oil particles via electrostatically and/or by van der Waals forces [46]. Chitosan selfassembled colloidal particles or composites with other natural polymers have been widely explored [49,50], and has shown significant potential across various applications [51], especially CS−based three-dimensional porous absorption materials [52]. However, weak point of the CS-based material for oil-absorbing materials is caused from inherently low mechanical strength. Therefore, improving chemical stability of the CS−based is essential for practical applications [53,54]

In this work, a natural oil/water absorbents SF, CS and SF/CS blended microparticles were fabricated via water-in-oil (W/O) emulsification-diffusion method. The chemical structure, morphology and thermal properties of the prepared absorbents were systematically characterized, and their oil-water absorption capacity was studied. Moreover, the crystallinity, hydrophobicity according to the shape as well as the interaction between SF and CS were also described and discussed.

2. Materials and Methods

2.1. Materials

The Thai silk *B. mori* cocoons (Nang Lai variety) was derived from the Silk Innovention Center (SIC), Mahasarakham University, Khamriang sub−district, Kantharawichai, Maha Sarakham, Thailand. Sodium carbonate (Na_2CO_3), calcium chloride ($CaCl_2$) was supplied by Elago Enterprises Pty Ltd. (New South Wales, Australia), and ethanol (C_2H_5OH), and chitosan from shrimp shells Chitosan (degree of deacetylation >85 %, Mw 30−50 kDa) were purchased from Merck KGaA company (Darmstadt, Germany). Acetic acid (CH_3COOH) was purchased from RCI Labscan Limited (Bangkok, Thailand). None of the reagent-grade chemicals used in this study needed to be further purified before being used.

 doi:10.20944/preprints202605.0850.v1

2.2. Preparation of Chitosan Solution

A 2 % (w/v) chitosan (CS) solution was prepared by dissolving the CS powder in a 1 % (v/v) acetic acid solution for 24 h. The CS solution was then adjusted to pH 6.5 using 1 M NaOH to form a CS microparticles.

2.3. Preparation of Silk Fibroin Solution

The *B. mori* cocoons were collected, cleaned, and then cut into small pieces. Then, boiled twice at 100°C for 30 minutes each in a 0.5% (w/v) Na_2CO_3 solution to remove silk sericin glue-like protein. After rinsing with distilled water until the pH was neutral, the degummed silk fibers were then immersed in a tertiary solvent system consisting of $CaCl_2$:Ethanol:H2O (1:2:8 by mol) for 60 minutes at 75°C while stirring constantly to give the SF solution. To remove any salt, the hydrolysate SF was dialyzed against distilled water for three days using a dialysis membrane (Thermo Scientific, Massachusetts, USA). Next, the SF solution's concentration was determined and adjusted to 1% (v/v) before use.

2.4. Preparation of SF, CS and SF/CS Blended Microparticles

All microparticles in this work were created by using the water−in−oil (W/O) emulsification diffusion method. Ethyl acetate was represented as an oil (O) phase, while the polymer (SF, CS and SF/CS) solutions were acted as a water (W) phase. Scheme 1 described on preparation of SF, CS and SF/CS solutions. It is already known that different form, size, and characteristics were influenced by volume, concentration, rate of stirring, and W:O ratios [55]. The condition being used for the particle construction was stirring rate in the range of 600−800 rpm, concentrations at 0.25−1.00% (w/v), and 100 ml of oil phase. In the preparation step, ethyl acetate as the oil phase was firstly contained in a container with stirred on the magnetic stirrer apparatus. A suitable volume of each polymer solution was then gentle added dropwise into the oil phase with stirring continued for 30 min. The formed particles were collected by dropper, and then placed into an eppendorf. Afterwards the particles were separated by centrifugation. The tubes were left at room temperature in a vacuum oven until the ethyl acetate was completely evaporated. In addition, the SF/CS blend microparticles were also constructed by the same method described above. The various SF/CS blend ratios of 3/1, 1/1, and 1/3 (v/v) from the optimal condition of each solution was selected. Before start, the blending solution was priorly mixed and stirred for 30 min to obtain homogeneous solutions. Aluminum foil was placed over the container in order to prevent the solvent from evaporating throughout the emulsification and diffusion processes. The construction of microparticle process is shown in Scheme 2.

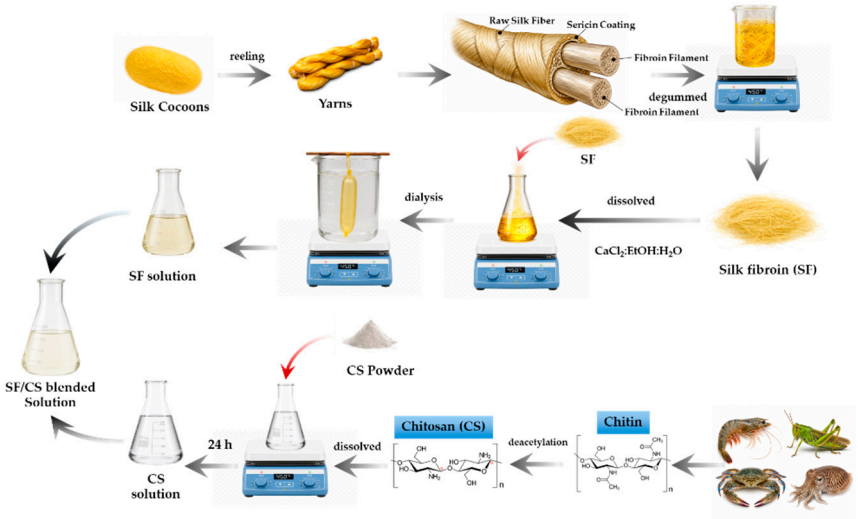

Scheme 1. shows diagram for SF, CS and SF/CS preparation.

 doi:10.20944/preprints202605.0850.v1

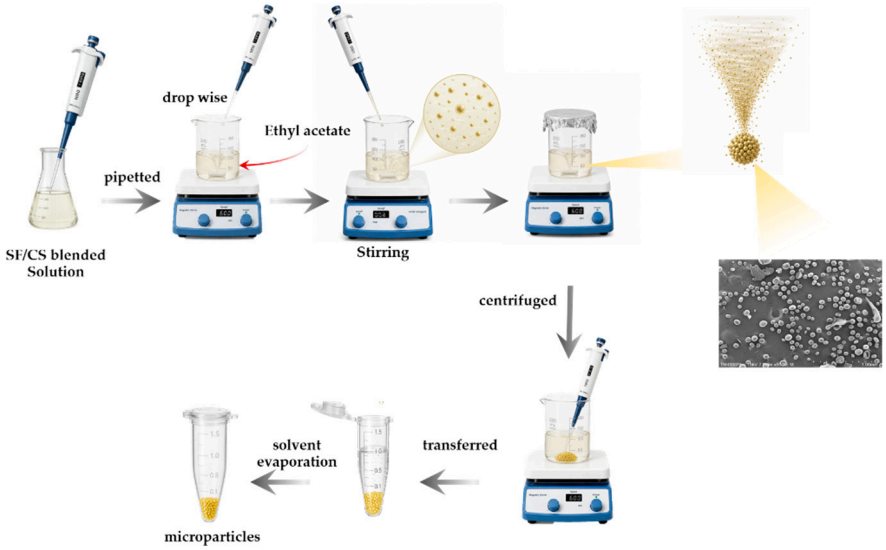

Scheme 2. shows diagram for microparticle preparation.

2.5. Characterization of the Microparticles

2.5.1. Morphology Observation

The microparticles were prepared according to the method described in Section 2.4. The samples were fixed onto a metal carrier stage with conductive adhesive and subjected to ion sputtering for gold coating. The microstructure of the samples was observed using a scanning electron microscope (SEM) (Hitachi, TM4000Plus, Tokyo, Japan) at an accelerating voltage of 15 kV.

2.5.2. Analysis of Interactions

The interactions among SF and CS in the microparticles were investigated using Fourier transform infrared (FTIR) spectrometer (Perkin Elmer-Spectrum Gx, USA) equipped with an attenuated total reflectance (ATR) accessory was applied. The results of the ATR-FTIR spectrum were obtained using 32 accumulated scans and the spectral range was 4000–400 cm^{-1} with a resolution of 4 cm^{-1}. This process was managed by using air as the reference. The microparticle samples were mixed with potassium bromide, ground into a fine powder, and pressed into pellets for FTIR analysis.

2.5.3. Thermal Stability

The thermal stability of the constructed microparticles was investigated using a thermogravimetric analyzer (TGA) (SDTQ600, TA−Instrument Co. Ltd., New Castle, DE, USA). The microparticles were placed within an aluminum pan before heating in the range of 50 to 700 °C by fixing a rate of 20 °C per minute. The condition of the process was performed in a nitrogen environment. The decreases in weight were recorded at several points in time.

2.5.4. Solubility Test

The solubility of the microparticles were tested according to previous report [56]. They were dried at 100 °C until the measured weight is constant (W_o). The test samples were placed into a test tube containing 5 mL of distilled water and then left at room temperature for 24 h. After the duration of 1, 3, 5 and 7 days, the non-solubilized particles were dried in an oven for 24 h and weighed (W_f). The measurements were done in triplicates for each duration. The dissolution (%) values were calculated using the following equation (1).

$$\text{Dissolution (\%)} = [(W_o - W_f)/ W_o] \times 100 \quad (1)$$

2.5.5. X−Ray Diffraction Analysis

 doi:10.20944/preprints202605.0850.v1

X−ray diffraction (XRD, Bruker D8, Germany) was used to characterize the prepared microparticles. The diffraction angle changed with a step size of 0.02°/s, ranging from 2θ = 5° to 60° with Cu Kα, λ = 1.5406 Å, 40 kV and 40 mA.

2.5.6. Oil Absorption Capacity

The microparticles were tested for chloroform, plant and used engine oil followed by previous report [57]. The tested microparticles were placed in a container with 2-mm-deep oil for 1 h to absorb oil, which then was moved to a sieve for separating the excess oil. The oil absorption capacity (OAC) was calculated by Equation (2):

$$OAC\ (g/g) = Mo \times Ma/Ma \quad (2)$$

where Mo and Ma represent the mass of oil−absorbed microparticles and original microparticles, respectively.

3. Results and Discussion

3.1. Morphological Studies

3.1.1. CS Microparticles

Previous reports have shown that there are several factors; volume of polymer, stirring rate, the water (W) to oil (O) phase ratio, and surfactants or crosslinking agents that affect the formation of spherical shapes in materials prepared using the water-in-oil-emulsification diffusion method [55,58,59]. The spherical shape of the microparticles has several advantages, especially the surface that comes into contact with the substance to be absorbed as well as released direction [59,60]. Figure 1 illustrates the morphology of the 1% CS microparticles that were created. The prepared microparticles have a size in the range of 60−100 μm. Under low magnification (Fig. 1a,b), the microparticles have a relatively uniformed size and are spherical. When the magnification is increased (Fig. 1c), the surface of the microparticles is smooth, with no roughness or cracks visibles and also packed closely. This might be suggested that the inside structure of CS formed chemical bond together [55]. When considering the maximum magnification (Fig. 1d), voids appear distributed within the microparticles, and there are small holes on the surfaces of the particles. This characteristic is believed to be caused by the water evaporation [61], which was the solvent used in preparing the CS solution.

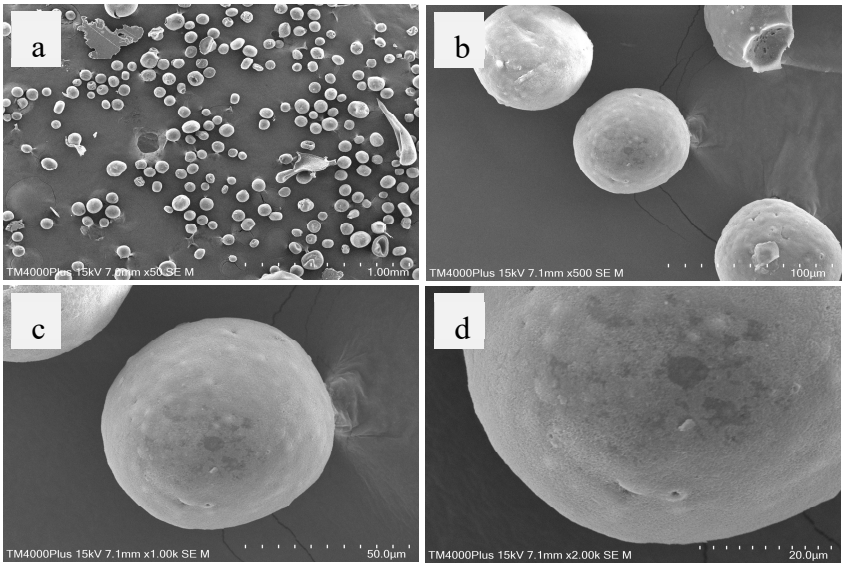

Figure 1. SEM micrographs of CS microparticles under different magnifications; 50X (a), 500X (b), 1000X (c), and 2000X (d), respectively.

 doi:10.20944/preprints202605.0850.v1

3.1.2. SF Microparticles

Figure 2 shows an SEM micrograph of the SF microparticles. Generally, the selected SF microparticles have a spherical shape with smooth surfaces and solid texture (Fig. 2a). However, in this time, preparing the SF microparticles to have a spherical shape is difficult. The shapes obtained are mostly incomplete, resulting in various forms such as thin sheets, lumps, or porous particles. These characteristics are expected to result from using old silkworm cocoons to prepare a silk fibroin solution. The structure or arrangement of amino acids in the silk protein may be damaged or altered, affecting the formation of chemical bonding or spherical shape when compared to previous experimental results [55,58,60]. When compared with CS microparticles, SF microparticles are approximately 1.5 times larger, ranging from 120 to 150 μm. With higher magnification as shown in Figure 2b, the surface of particles exhibits numerous small pores evenly distributed covering all surface area. It is believed that these pores are formed by the evaporation of water during the particle preparation process. The evaporation of water causes the SF molecules to come closer together, resulting in the formation of chemical bonds. These bonds resulted in the particle harder and solid [62,63].

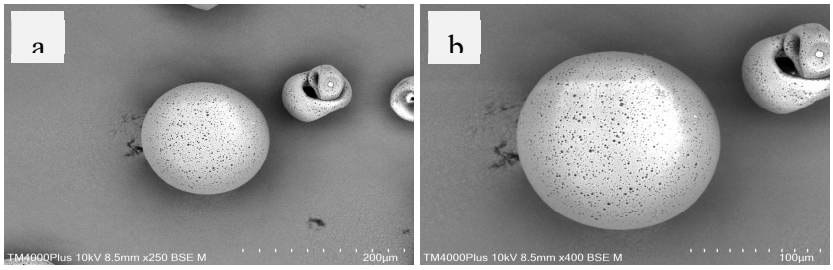

Figure 2. SEM micrographs of SF microparticles with different magnifications; 250X (a), and 400X (b), respectively.

3.1.3. SF/CS Blended Microparticles

The SF/CS blended microparticles were prepared using 1% (w/v) CS solution and 1% SF solution with different volume ratios of 3:1, 1:1, and 1:3, respectively. Figure 3 shows the SF/CS blended microparticles at a 3:1 ratio. At low magnifications (Fig. 3a,b), the shape of the microparticles obtained fromthis ratio are not spherical, irregular form, indentations, and have a comparatively smooth surface. Particular sizes range from 30 to 60 μm on everage. However, the particle preparation is found to be modest and incomplete at this ratio. This might be caused from the greater SF ratio, which prevent the the creation of entire particles. SF would be packed together before interaction to CS. Comparison to the pure SF microparticles (Fig. 2), the CS helps in the particles◎more thorough formation. It can be seen that the surface of the microparticles is rough due to the unevenness of the surface aria when considered under high magnification (Fig. 3c).

Figure 4 shows the SF/CS blended microparticles at a 1:1 ratio. The average particle size is range from 20 to 60 μm on everage. Under low magnification (Figure 4a), it can be seen that the prepared microparticles have different shapes; rod, round, flat, ellipse, and incomplete round shape. At high magnifications (Fig. 4b,c), the microparticles are relatively complete, with some pores on the surface. This pore caused by polar components of the microparticle which evaporated during drying [64]. The obtained results also indicated that addition of CS helps to form more complete particles compared to pure SF.

Figure 5 shows the SF/CS blended microparticles at a 1:3 ratio. It can be seen that the prepared particles are spherical, well−formed, and have a relatively smooth surface. The average size of microparticles is between 60 to 80 μm (Fig. 5a, b). Generally, a large number of spherical

 doi:10.20944/preprints202605.0850.v1

microparticles can be prepared from this ratio. However, it is found that the surface of the microparticles has a wavy texture when observed at high magnification (Fig. 5c). This is believed to be due to the difference polarity between the SF and CS, resulting in an uneven compatibility.

Previous report suggested that the size and shapes of the blended microparticles affecting by several factors, particularly the polymer chain, which derived from the preparation process. Additionally, if different types of polymers are used, the blending ratio is another factor [55,65].

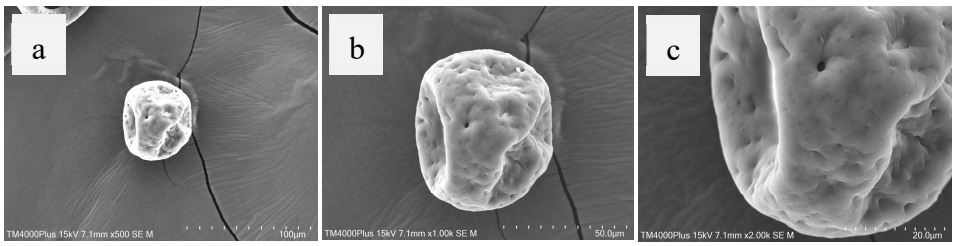

Figure 3. SEM micrographs of SF/CS (3:1) blended microparticles with different magnifications; 500X (a), 1000X (b), and 2000X (c), respectively.

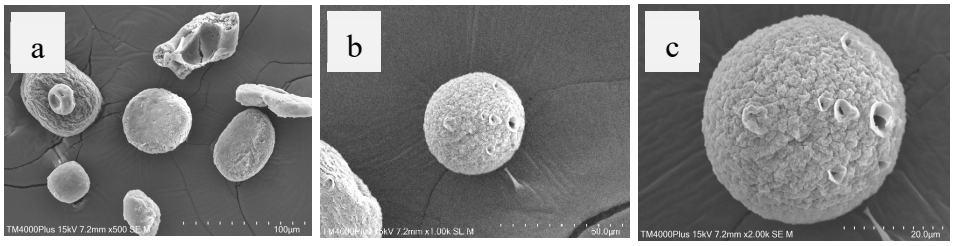

Figure 4. SEM micrographs of SF/CS (1:1) blended microparticles with different magnifications; 500X (a), 1000X (b), and 2000X (c), respectively.

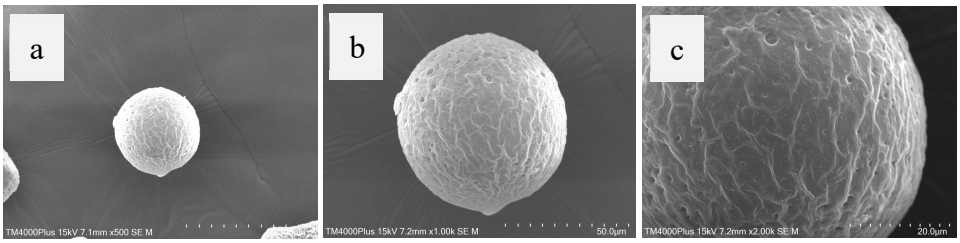

Figure 5. SEM micrographs of SF/CS (1:3) blended microparticles with different magnifications; 500X (a), 1000X (b), and 2000X (c), respectively.

3.2. Water Solubility

The water solubility values (% weight loss) for the prepared microparticles as shown in Table 1. The results found that all prepared microparticles could be existed in water over seven days, which indicated the stability of the microparticles. At final time, all microparticles remained their weight in over 75 percentages. Among types, SF and SF/CS blended at 3:1 and 1:3 showed rapidly degraded starting on day 3, and then gradualy loose their weight until the end of experimental test. CS microparticles show strong stability in water. This due to CS, generally, non−degraded in water. SF/CS blended at 1:1 also found to stable in water. This suggested that this ratio supported the chemical bonding formation between both materials, enhances water solubility [66].

Table 1. Summarize the water solubility of different types of microparticles.

 doi:10.20944/preprints202605.0850.v1

Types	Dissolution Time (days)				
	0	1	3	5	7
Native SF	100 ± 0.00	100 ± 0.00	90.00 ± 3.00	85.00 ± 2.00	80.00 ± 3.00
SF/CS (3:1)	100 ± 0.00	100 ± 0.00	88.00 ± 2.00	82.00 ± 2.00	75.00 ± 2.00
SF/CS (1:1)	100 ± 0.00	100 ± 0.00	90.00 ± 3.00	85.00 ± 4.00	80.00 ± 2.00
SF/CS (1:3)	100 ± 0.00	100 ± 0.00	86.00 ± 2.00	80.00 ± 2.00	76.00 ± 1.00
Native CS	100 ± 0.00	100 ± 0.00	92.00 ± 3.00	84.00 ± 4.00	79.00 ± 3.00

3.3. Functional Groups Analysis

ATR−FTIR spectroscopy popularly used for functional groups analysis. Figure 6a shows the absorption peaks of SF microparticles. The specific region of protein is peptide bonds, where amino acids are bonded to one another. This location is called "amide types" composed of amide I (1700−1600 cm^{-1}), amide II (1600−1500 cm^{-1}), and amide III (1300−1200 cm^{-1}) [55,67,68]. The three different types of amides are related to the secondary structure of the protein, such as α−helix or β−pleated sheet. From the spectra, amide I (C=O stretching), with absorption regions including 1640 cm^{-1} (α−helix), 1620−1640 cm^{-1} (β−turns), and 1645 cm^{-1} (random coil). Additionally, there are amide II (N−H bending and C−N stretching) at 1558 cm^{-1} and amide III (C−N and N−H bending) at 1325 cm^{-1} [69,70].

The CS microparticles (Fig. 6e) exhibit absorption in the range of 3291-3361 cm^{-1}, which corresponds to the N−H and O−H stretching groups, as well as the positions of hydrogen bonds formation within the molecule. The absorption positions at approximately 2921 and 2877 cm^{-1} are due to C−H stretching and asymmetric stretching, respectively. All these absorption positions are specific to polysaccharides, which are also commonly found in other polysaccharides such as xylan [71], glucan [72], and carrageenan [73]. The spectrum also shows the N−acetyl group at 1645 cm^{-1} (C=O stretching of amide I) and 1325 cm^{-1} (C−N stretching of amide III), respectively. However, the absorption peak around 1550 cm^{-1}, which is the specific absorption region for N−H bending of amide II and is also characteristic of N−acetyl groups, is not observed. Generally, this position is overlapped by other groups. An absorption peak at 1589 cm^{-1} is observed, which corresponds to the N−H bending of amine groups [74]. Additionally, there are two more absorption peaks at 1423 and 1375 cm^{-1}, which correspond to the $-CH_2$ bending and the symmetric stretching of $-CH_3$ groups, respectively. The absorption band at 1153 cm^{-1} corresponds to the asymmetric stretching of the glycosidic bond (C−O−C linkage), and the absorption regions at 1066 and 1028 cm^{-1} correspond to the C−O stretching groups. All the mentioned absorption regions indicate the structure of chitosan that has been previously reported [75−77].

The SF/CS blended microparticles at a ratio of 3:1 (Fig. 6b) exhibits an overall are the absorption characteristic like both pure SF and CS microparticles. However, slight differences in absorption are observed, particularly in the absorption regions at 3700 cm^{-1} and 1158−1167 cm^{-1}. These differences are expected to arise from interactions between the functional groups of the SF (C=O, N−H) and CS (N−H, O−H, C−O−C) via hydrogen bonds and electrostatic interactions.

Figure 6c shows the absorption peaks of SF/CS blended microparticles at a 1:1 ratio. The peaks associated with SF begin to decrease, while the peaks of CS become more dominant (3700−3720 cm^{-1}, and 1158−1167 cm^{-1}). However, at the absorption position around 1580 cm^{-1}, there is a clear shift toward lower absorption values. This indicates that the amine groups ($-NH_2$) of CS are transforming into amide II (−NH) of SF, as well as the formation of bonds between the hydroxyl groups (−OH) of CS and the peptide positions of SF.

Figure 6d shows the absorption peaks of SF/CS blended microparticles at a 1:3 ratio. The absorption pattern like that of CS, particularly in the regions at 1620−1630 cm^{-1} (C=O group), 100−1100 cm^{-1} (asymmetric position by β−(1−4) glycosidic bonds) [78], and 1560 cm^{-1} (−NH group). The shift in the absorption regions is due to the chemical bonding formation between SF and CS. Details of the absorption peaks of the functional groups are summarized in Table 2.

 doi:10.20944/preprints202605.0850.v1

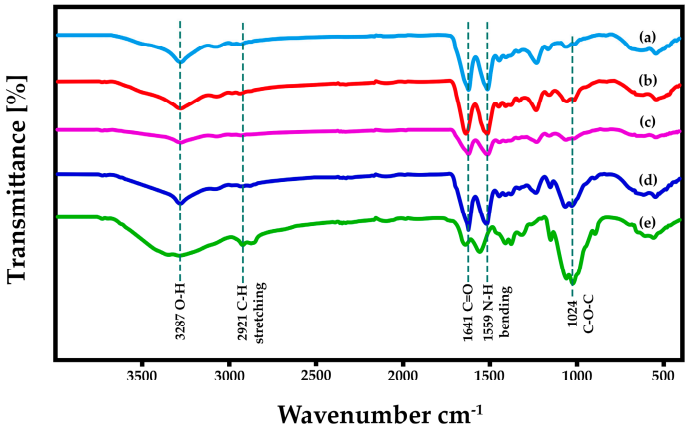

Figure 6. ATR-FTIR spectra of microparticles; native SF (a), SF/CS blended at 3:1 (b), 1:1 (c), and 1:3 (v/v) (d) ratios, and native CS (e).

Table 2. Summarize the adsorption peaks in the FTIR spectra of different types of microparticles.

Types	Absorption (cm^{-1})				
	O–H Str.	C–H Str.	C=O Str.	N–H Str.	C–O Blend
Native SF	3290	2921	1641	1558	-
SF/CS (3:1)	3290	2928	1642	1559	1024
SF/CS (1:1)	3290	2956	1623	1559	1024
SF/CS (1:3)	3290	2956	1624	1559	1024
Native CS	3291	2921	1645	1589	1024

3.4. Weight Loss Analysis

Figure 7 shows the TG curves of all the prepared microparticles. The microparticles undergo degradation in at least two stages: the first stage occurs at approximately 100 °C, where the weight of the microparticles decreases slightly due to the evaporation of water molecules [79]. The second stage occurs at temperatures between 300–400 °C, which is the degradation of the main polymer structure [62,63,80]. CS microparticles are more resistant to degradation than other particles. At the maximum temperature test, the weight of microparticles remains about 25% (charred residues). The remaining substances are carbon that cannot be degraded [55]. The charred residue of the blended microparticles remains similar content to native SF at the end temperature test. The native CS microparticle had the highest charred residue. Moreover, the native CS microparticle had a greater stability to heat than other microparticles. The maximum temperature decomposition ($T_{d, max}$) could be detailed in the DTG curves as shown in Figure 8. Table 3 provides the microparticle's decomposition. The values of T5%, T10%, and T50% of native CS microparticles are higher than native SF microparticles. This indicated that the SF microparticles absorbed water higher than CS microparticles. In case of SF/CS blended, 1:1 ratio shows highest values. It is suggested that this ratio might be formed chemical bonding between SF and CS, resulting in decrease water absorption [55,81,82]. However, the value of T5%, T10% SF/CS blended at 1:3 higher than SF/CS blended at 3:1. The results revealed that at low temperature, the SF/CS blended at 3:1 rapidly decomposed but slowly decomposed at higher temperature. The $T_{d, max}$ of the SF/CS blended microparticles increased following the SF content.

 doi:10.20944/preprints202605.0850.v1

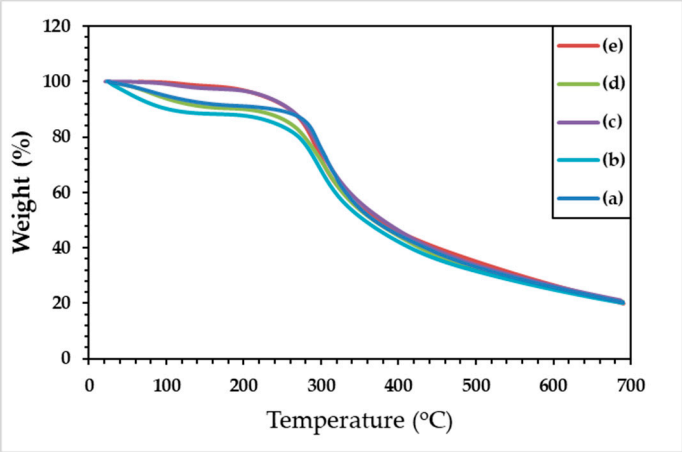

Figure 7. TG curves of microparticles; native SF (a), SF/CS blended at 3:1 (b), 1:1 (c), and 1:3 (v/v) (d) ratios, and native CS (e).

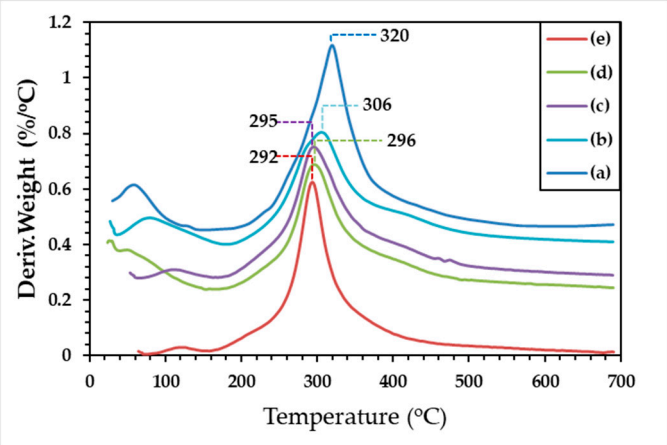

Figure 8. DTG curves of microparticles; native SF (a), SF/CS blended at 3:1 (b), 1:1 (c), and 1:3 (v/v) (d) ratios, and native CS (e).

Table 3. Thermal decomposition properties of different microparticles.

Types	Thermal decomposition (°C)				[1]Charred residues (%)
	[1]$T_{5\%}$	[1]$T_{10\%}$	[1]$T_{50\%}$	[2]T_{max}	
Native SF	98	238	386	320	28
SF/CS (3:1)	88	201	387	312	29
SF/CS (1:1)	224	260	401	300	29
SF/CS (1:3)	221	253	373	297	29
Native CS	222	259	424	294	30

[1]Obtained from TG thermograms. [2]Obtained from DTG thermograms.

3.5. Crystallinity Determination

Crystaline structure of the microparticles was analyzed using X−ray Diffraction (XRD), by scanning in the 2θ range of 5−60°. As shown in Figure 9, it was found that all the prepared microparticles exhibited XRD signals characteristic of a semi-crystalline polymer, within the main peaks appearing at approximately 11.9° and 20.6° (Fig. 9). These peaks are specific to the β−sheet structure of SF [55]. In addition, broad peaks were observed at approximately 20°, which are associated with the crystalline regions of CS [83,84]. The SF/CS blended microparticles at different ratios (Fig. 9b,c,d), sharper and more intense peaks gradually inclined to CS depending on CS ratios.

 doi:10.20944/preprints202605.0850.v1

This suggested that the crystallinity of the blended microparticles is dependent on both SF and CS contents. Generally, chitosan is a semicrystalline polymers. The preparation process, form as well as intermolecular H−bonging are main factors on its crystalline structure. When blending SF, the SF/CS microparticles revealed sharp and more intense peak signals, indicating an increase in the degree of crystallinity. The hydrophobic parts in SF structure might be form β−sheet structure and promote the formation of hydrogen bonds between the amino groups of SF and the hydroxyl groups of CS [85].

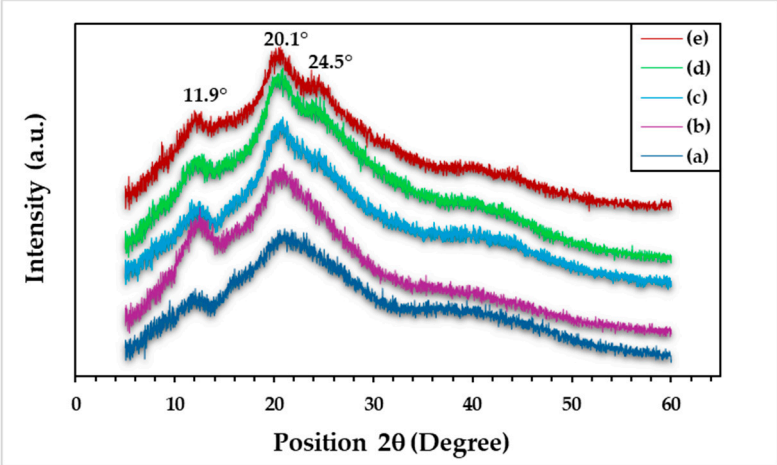

Figure 9. XRD patterns of microparticles; native SF (a) SF/CS blended at 3:1 (b), 1:1 (c), and 1:3 (v/v) (d) ratios, and native CS (e).

3.6. Absorption Capacity Test

The results of the absorption efficiency test of the prepared microparticles, using the absorption samples of chloroform, vegetable oil, and used engine oil, are shown in Table 4. Upon detailed examination, it was found that both SF and CS microparticles had the lowest capacity to absorb chloroform. SF microparticles could absorb used engine oil more than the other microparticles, while CS microparticles could absorb vegetable oil slightly more than used engine oil. The SF/CS blended microparticles exhibited varying adsorption capacities. The capacity of the blended microparticles depends on the ratio of the polymer used for preparation [86]. However, it can be suggested that the blended microparticles' ability to absorb used engine oil decreases with a lower ration of SF. In contrast, an increase in capacity to absorb vegetable oil enhances by CS amount [87]. The results indicated that the hydrophobicity of SF directly affects absorption. It is well known that SF is composed of repeated units of small non-polar amino acids like glycine and alanine. These amino acids help to make directional arrangements to form crystalline part of SF structure. Additionally, it may be due to the different components in the oils. Mostly, vegetable oil is a triglyceride, whereas engine oil contains multiple components such as mineral oil and quality additives. These substances are all specific in their binding to different particles. The CS structure has many amino groups ($-NH_2$) that dissociate to form positive charge in acid condition, can create adhesive forces with the negatively charged molecules of vegetable oil at the carboxylic group. Moreover, the surface characteristics of the microparticles, such as roughness or inward concavity may increase the contact area, leading to higher absorption [88]. Therefore, it is expected that the SF/CS blended microparticles can be applied as oil absorbents in the environment when combined with other devices or materials.

Table 4. Absorption capacity of the different microparticles.

 doi:10.20944/preprints202605.0850.v1

Types	Absorption Capacity (g/g)		
	Chloroform	Plant Oil	Used Engine Oil
Native SF	1.90	11.50	17.90
SF/CS (3:1)	2.50	13.50	15.80
SF/CS (1:1)	3.80	20.85	21.53
SF/CS (1:3)	2.10	16.10	15.16
Native CS	1.70	15.33	14.00

4. Conclusions

The issue of oil contamination in water is considered one of the major global problems that affect ecosystems and aquatic life. Currently, there are several approaches to managing this issue, each with its own advantages, such as bioremediation, chemical dispersants, and physical removal techniques. However, researchers have been continuously seeking new methods to help remove oil from water, such as bioremediation techniques, advanced filtration systems, and the use of absorbent materials that can effectively capture and eliminate oil pollutants. This work aims to prepare oil-absorbing particles from fibroin and chitosan, which are natural materials reported to absorb non-polar substances, including oil, using the water−in−oil−emulsification diffusion technique. Under SEM, the SF microparticles were the largest, followed by CS and the SF/CS blended microparticles, respectively. The CS microparticles had a spherical shape and smooth surface, unlike the SF microparticles, which had a non-spherical shape and less smooth surface compared to the CS microparticles. The SF/CS blended microparticles had a shape that varied according to the ratio used. All the prepared particles were resistant to dissolution in water by more than 75% when tested for a week. By FTIR spectra, SF and CS microparticles exhibit absorption peaks of functional groups characteristic of proteins and polysaccharides, as well as main structural bonds. Some peaks in the blended microparticles were shifted, indicating the formation of chemical bonds between SF and CS. Chemical bonds, such as hydrogen bonds and electrostatic interactions, lead to increased crystallinity and thermal properties of the composite particles, as observed by XRD and TGA analysis. When testing the absorption, it was found that all the prepared particles absorbed the least amount of chloroform. The SF microparticles absorbed more used engine oil than vegetable oil, while the CS microparticles absorbed the most vegetable oil. This indicates that the particles prepared from SF and CS might potentially be used for oil absorption. However, the type of adsorbent and oil still need to be considered before practical use. In the future, systematic studies on the kinetics of oil adsorption of SF and CS microparticles, as well as the enhancement of oil adsorption capacity through mixing with other materials would be studied. In addition, modifying the structure of materials containing SF and CS need to be conducted to enable their effective use as oil adsorbents.

Author Contributions: Conceptualization, A.T. and P.S.; methodology, W.S. and P.S.; investigation, S.T. and P.S.; resources, S.T., A.T.; visualization, S.T., Y.B. and P.S.; writing-original draft, A.T., P.S., and W.S.; writing, reviewing, and editing, A.T., P.S., and Y.B. After reading the published version of the manuscript, all writers have given their approval.

Funding: This research project was financially supported by Thailand Science Research and Innovation (TSRI). The Center of Excellence for Innovation in Chemistry (PERCH-CIC), Office of the Higher Education Commission, Ministry of Education, Thailand, for its partial funding is also appreciated by P.S.

Data Availability Statement: Not applicable.

Conflicts of Interest: No conflicts of interest are disclosed by the authors.

 doi:10.20944/preprints202605.0850.v1

References

1. Duan, B.; Gao, H.; He, M.; Zhang, L. Hydrophobic modification on surface of Chitin Sponges for Highly Effective Separation of Oil. *ACS Appl. Mater. Interfaces*, **2014**, *6*, 19933–19942.
2. Chen, C.; Zhu, X.; Chen, B. Durable Superhydrophobic/Superoleophilic Graphene-based Foam for High-Efficiency Oil Spill Cleanups and Recovery. *Environ. Sci. Technol.* **2019**, *53*, 1509–1517.
3. Zhou, J.; Zhang, Y.; Yang, Y.; Chen, Z.; Jia, G.; Zhang, L. Silk Fibroin-Graphene Oxide Functionalized Melamine Sponge for Efficient Oil Absorption and Oil/Water Separation. *Appl. Surf. Sci.* **2019**, *497*, 143762.
4. Duan, H.; Lyu, H.; Shen, B.; Tian, J.; Pu, X.; Wang, F.; Wang, X. Superhydrophobic-Superoleophilic Biochar-based Foam for High-Efficiency and Repeatable Oil-Water Separation. *Sci. Total Environ.* **2021**, *780*, 146517.
5. Xu, C.; He, H.; Wang, Y.; Huang, Y.; Zhang, T.C.; Yuan, S. Superhydrophobic Sponge-like Chitosan/CNTs/Silica Composite for Selective Oil Absorption and Efficient Separation of Water-in-Oil Emulsion. *Carbohyd. Polym.* **2025**, *353*, 123256.
6. Riehm, D.A.; Neilsen, J.E.; Bothun, G.D.; John, V.T.; Raghavan, S.R.; McCormick, A.V. Efficient Dispersion of Crude Oil by Blends of Food-Grade Surfactants: Toward Greener Oil-Spill Treatments. *Mar. Pollut. Bull.* **2015**, *101*, 92–97.
7. Motta, F.L.; Stoyanov, S.R.; Soares, J.B.P. Application of Solidifiers for Oil Spill Containment: A Review. *Chemosphere* **2018**, *194*, 837–846.
8. Owoseni, O.; Nyankson, E.; Zhang, Y.; Adams, S.J.; He, J.; McPherson, G.L.; Bose, A.; Gupta, R.B.; John, V.T. Release of Surfactant Cargo from Interfacially-Active Halloysite Clay Nanotubes for Oil Spill Remediation. *Langmuir* **2014**, *30*, 13533–13541.
9. Xiao, J.; Lv, W.; Song, Y.; Zheng, Q. Graphene/nanofiber aerogels: performance reg ulation towards multiple applications in dye adsorption and oil/water separation. *Chem. Eng. J.* **2018**, *338*, 202–210.
10. Yang, Y.; Ren, Z.; Zhao, S.; Guo, Z. One-Step Fabrication of Thermal Resistant, Corrosion Resistant Metal Rubber for Oil/Water Separation. *Colloids Surf. A Physicochem. Eng. Asp.* **2019**, *573*, 157–164.
11. Yu, T.; Swientoniewski, L.T.; Omarova, M.; Li, M.C.; Negulescu, I.I.; Jiang, N.; Darvish, O.A.; Panchal, A.; Blake, D.A.; Wu, Q.; Lvov, Y.M.; John, V.T.; Zhang, D. Investigation of Amphiphilic Polypeptoid-Functionalized Halloysite Nanotubes as Emulsion Stabilizer for Oil Spill Remediation. *ACS Appl. Mater. Interfaces* **2019**, *11*, 27944–27953.
12. Aurell, J.; Gullett, B.K. Aerostat Sampling of PCDD/PCDF Emissions from the Gulf Oil Spill In Situ Burns. *Environ. Sci. Technol.* **2010**, *44*, 9431–9437.
13. Abidli, A.; Huang, Y.; Cherukupally, P.; Bilton, A.M.; Park, C.B. 2020. Novel Separator Skimmer for Oil Spill Cleanup and Oily Wastewater Treatment: from Conceptual System Design to the First Pilot-scale Prototype development. *Environ. Technol. Innov.* **2020**, 100598.
14. Kristensen, M.; Johnsen, A.R.; Christensen, J.H. Marine Biodegradation of Crude Oil in Temperate and Arctic Water Samples. *J. Hazard. Mater.* **2015**, *300*, 75–83.
15. Wang, J.; Sandoval, K.; Ding, Y; Stoeckel, D.; Minard-Smith, A.; Andersen, G.; Dubinsky, E.A.; Atlas, R.; Gardinali, P. Biodegradation of dispersed Macondo crude oil by indigenous Gulf of Mexico micro bial communities. *Sci. Total Environ.* 2016, 557-558, 453–468.
16. Hoang, A.T.; Nižetić S.; Duong, X.Q.; Rowinski, L.; Nguyen, X.P. Advanced Super-Hydrophobic Polymer Based Porous Absorbents for the Treatment of Oil-Polluted Water. *Chemosphere*, **2021**, *277*, 130274.
17. Zhou, X.; Zhang, Z.; Xu, X.; Men, X.; Zhu, X. Facile Fabrication of Superhydrophobic Sponge with Selective Absorption and Collection of Oil from Water. *Ind. Eng. Chem. Res.* **2013**, *52*, 9411–9416.
18. Ge, J.; Wang, F.; Yin, X.; Yu, J.; Ding, B. Polybenzoxazine-Functionalized Melamine Sponges with Enhanced Selective Capillarity for Efficient Oil Spill Cleanup. *ACS Appl. Mater. Interfaces* **2018**, *10*, 40274–40285.
19. Li, J.; Chen, Y.; Gao, J.; Zuo, Z.; Li, Y.; Liu, H.; Li, Y. Graphdiyne Sponge for Direct Collection of Oils from Water. *ACS Appl. Mater. Interfaces* **2018**, *11*, 2591–2598.
20. Phanthong, P.; Reubroycharoen, P.; Kongparakul, S.; Samart, C.; Wang, Z.; Hao, X.; Abudula, A.; Guan, G. Fabrication and Evaluation of Nanocellulose Sponge for Oil/Water Separation. *Carbohydr. Polym.* **2018**, *190*, 184–189.

 doi:10.20944/preprints202605.0850.v1

21. Sam, E.K.; Liu, J.; Lv, X. Surface Engineering Materials of Superhydrophobic Sponges for Oil/Water Separation: A Review. *Ind. Eng. Chem. Res.* **2021**, *60*, 2353–2364.
22. Sarkar, A.; Mahapatra, S. Novel Hydrophobic Vaterite Particles for Oil Removal and Recovery. *J. Mater. Chem. A* **2014**, *2*, 3808−3818.
23. Gao, C.; Xing, Z.; Chen, Y.; Meng, L.; Tang, X. Improve the Chitosan Particle-Stabilized Oil-Water Interface by Dual Reinforcement and Its Effect on the Structure and Properties of Emulsion. *Food Chem.* **2025**, *485*, 144500.
24. Yang, Y.; Tong, Z.; Ngai, T.; Wang, C. Nitrogen-Rich and Fire Resistant Carbon Aerogels for the Removal of Oil Contaminants from Water. *ACS Appl. Mater. Interfaces* **2014**, *6*, 6351−6360.
25. Li, Y.-Q.; Samad, Y. A.; Polychronopoulou, K.; Alhassan, S. M.; Liao, K. Carbon Aerogel from Winter Melon for Highly Efficient and Recyclable Oils and Organic Solvents Absorption. *ACS Sustainable Chem. Eng.* **2014**, *2*, 1492−1497.
26. Wang, Q.; Li, Y. Facile and Green Fabrication of Porous Chitosan Aerogels for Highly Efficient Oil/Water Separation and Metal Ions Removal from Water. *J. Envi. Chem. Eng.* **2023**, *11*, 109689.
27. Wang, Y. ; Chen, A.; Peng, M.; Tan, D.; Liu, X.; Shang, C.; Luo, S.; Peng, L. Preparation and Characterization of a Fluorizated Kaolin–Modified Melamine Sponge as an Absorbent for Efficient and Rapid Oil/Water Separation. *J. Clean. Prod.* **2019**, *217*, 308–316.
28. Xia, C.; Li, Y.; Fei, T.; Gong, W. Facile One-Pot Synthesis of Superhydrophobic Reduced Graphene Oxide-Coated Polyurethane Sponge at the Presence of Ethanol for Oil-Water Separation. *Chem. Eng. J.* **2018**, *345*, 648–658.
29. Lin, X.; Li, Y.; Chen, Z.; Zhang, C.; Luo, X.; Du, X.; Huang, Y. Synthesis, Characterization and Electrospinning of New Thermoplastic Carboxymethyl Cellulose (TCMC). *Chem. Eng. J.* **2013**, *215–216*, 709–720.
30. Xiang, B.; Sun, Q.; Zhong, Q.; Mu, P.; Li, J. Current research situation and future prospect of superwetting smart oil/water separation materials. *J. Mater. Chem. A* **2022**, *10*, 20190–20217.
31. Wang, K.; Zhang, T.C.; Wei, B.; Chen, S.; Liang, Y.; Yuan, S. Durable CNTs Reinforced Porous Electrospun Superhydrophobic Membrane for Efficient Gravity Driven Oil/Water Separation. *Colloid. Surf. A: Physicochem. Eng. Asp.* **2021**, *608*, 125342.
32. Zhou, J.; Zhang, Y.; Yang, Y.; Chen, Z.; Jia, G.; Zhang, L. Silk Fibroin-Graphene Oxide Functionalized Melamine Sponge for Efficient Oil Absorption and Oil/Water Separation. *Appl. Surf. Sci.* **2019**, *497*, 143762.
33. Altman, G.H.; Diaz, F.; Calabro, C.T.J.; Horan, R.L.; Chen, J.; Lu, H.; Richmond, J.; Kaplan, D.L. Silk- Based Biomaterials. *Biomaterials* **2003**, *24*, 401–416.
34. Zhang, Y.Q. Applications of Natural Silk Protein Sericin in Biomaterials. *Biotechnol. Adv.* **2002**, *20*, 91–100.
35. Liu, Q., Liu, H., Fan, Y. Preparation of Silk Fibroin Carriers for Controlled Release. *Microsc. Res. Tech.* **2017**, *80*, 312–320.
36. Lyu, Y.; Liu, Y.; He, H.; Wang, H. Application of Silk-Fibroin-Based Hydrogels in Tissue Engineering. *Gels* **2023**, *9(5)*, 431.
37. Hu, J.; Jiang, Z.; Zhang, J.; Yang, G. Application of Silk Fibroin Coatings for Biomaterial Surface modification: a silk road for biomedicine. Journal of Zhejiang University-SCIENCE B (Biomedicine & Biotechnology) 2023 24(11):943-956.
38. Hu, Y., Zou, Y., Ma, Y., Yu, J., Liu, L., Chen, M., Ling, S., Fan, Y. Formulation of Silk Fibroin Nanobrush-Stabilized Biocompatible Pickering Emulsions. *Langmuir* 2022, 38, 14302−14312.
39. Hu, Y.; Ma, Y.; Liu, L.; Yu, J.; Cui, J.; Ling, S.; Fan, Y. Nanosilk Template-Guided/Induced Construction of Brush-/Flower-Like 3D Nanostructures. *ACS Appl. Mater. Interfaces* **2023**, *15*, 14654−14663.
40. Liu, Y.; Liu, L.; Li, X.; Yu, J.; Chen, M.; Lin, L.; Jia, R.; Fan, Y. Pickering Emulsions by Combining Nanocellulose/Nanochitin and Silk Fibroin: Silk Fibroin as a Stabilizer or an Emulsifier. *Ind. Crops Prod.* **2024**, *211*, 118270.
41. Han, X.; Ke, Y.; Wu, Y.; Huang, J.; Xu, W.; Wang, Y. Surface Modification of Silk Fibroin Powder and Its Application in Oil–Water Separation. *Pow. Technol.* **2023**, *420*, 118397.
42. Zong, C.-M.; Zhang, B.; Li, S.-Y.; Jin, J.; Lu, Z.-Z.; Yao, X.-H.; Zhao, W.-G.; Chen, T.; Zhang, D.-Y. A Flexible Multifunctional Sensor with a Conductive Network Based on Silk Nanofibers and MXene for Monitoring

 doi:10.20944/preprints202605.0850.v1

Physiological Activity, Capacitive Pens, Photothermal Conversion and Antibacterial. *Int. J. Biol. Macromol.* **2025**, *305*, 141148.

43. Xin, L.; Hu, Z.; Mao, Y.; Wu, G.; Chen, W.; Lu, W. Biocompatible Silk Nanofibers with Excellent Antimicrobial and Preservation Properties by ε-Polylysine Grafting. *Food Chem.* **2026**, *506*, 148204.
44. Abd-Elbaki, M.K.M.; Ahmed, R.M.G.; Khalil, A.S.G. Silk-based 2D Nanocomposites for Superior Oily Wastewater Remediation. *J. Clean Prod.* **2022**, *365*, 132707.
45. Gore, P.M.; Naebe, M.; Wang, X.; Kandasubramanian, B. Progress in Silk Materials for Integrated Water Treatments: Fabrication, Modification and Applications. *Chem. Eng. J.* **2019**, *374*, 437-470.
46. Kou, S.(Gabriel); Peters, L.; Mucalo, M. Chitosan: A Review of Molecular Structure, Bioactivities and Interactions with the Human Body and Micro-Organisms. *Carbohydr. Polym.* **2022**, *282*, 119132.
47. Hamid, M.; Dayana, I.; Sholeha, D.; Siregar, M.F.; Roza, I.; Junaidi, Rianna, M.; Wijoyo, H. Eco-Friendly Utilization of Chitosan from Shrimp Shells for Used Lubricating Oil Cleaning. *Res. Surf. Interfaces* **2025**, *18*, 100368.
48. Qian, J.; Yin, J.; Ma, P.; Mo, C.; Chen, Y.; Guo, H. Study on Emulsification Property of Chitosan with Strong Antibacterial Activity. *Food Hydrocoll.* **2026**, *179*, 112711.
49. Han, J.; Chen, F.; Gao, C.; Zhang, Y.; Tang, X. Environmental Stability and Curcumin Release Properties of Pickering Emulsion Stabilized by Chitosan/Gum Arabic Nanoparticles. *Int. J. Biol. Macromol.* **2020**, *157*, 202–211.
50. Zhang, N.; Han, J.; Chen, F.; Gao, C.; Tang, X. Chitosan/Gum Arabic Complexes to Stabilize Pickering Emulsions: Relationship Between the Preparation, Structure and Oil-Water Interfacial Activity. *Food Hydrocoll.* **2022**, *129*, 107532.
51. Meng, W.; Sun, H.; Mu, T.; Garcia-Vaquero, M. Chitosan-Based Pickering Emulsion: A Comprehensive Review on their Stabilizers, Bioavailability, Applications and Regulations. *Carbohydr. Polym.* **2023**, *304*, 120491.
52. Paul, J.; Qamar, A.; Ahankari, S.S.; Thomas, S.; Dufresne, A. Chitosan-Based Aerogels: A New Paradigm of Advanced Green Materials for Remediation of Contaminated Water. *Carbohydr. Polym.* **2024**, *338*, 122198.
53. Gao, C.; Xing, Z.; Chen, Y.; Meng, L.; Tang, X. Improve the Chitosan Particle-Stabilized Oil-Water Interface by Dual Reinforcement and Its Effect on the Structure and Properties of Emulsion. *Food Chem.* **2025**, *485*, 144500.
54. Rao, R.; Liu, M.; Yu, X.; Li, X.; Guo, X.; Shi, X. Antibacterial Chitosan Bioplastics with Enhanced Water Stability via Electro-Assembly Followed by Direct Thermal Processing. *Carbohydr. Polym.* **2026**, *381*, 125190.
55. Tanisood, S.; Baimark, y.; Srihanam, P. Preparation and Characterization of Cellulose/Silk Fibroin Composite Microparticles for Drug-Controlled Release Applications. *Polymers* **2024**, *16*, 3020.
56. Rojas-Lema, S.; Nilsson, K.; Trifol, J.; Langton, M.; Gomez-Caturla, J.; Balart, R.; Garcia-Garcia, D.; Morina, R. Faba Bean Protein Films Reinforced with Cellulose Nanocrystals as Edible Food Packaging Material. *Food Hydrocoll.* **2021**, *121*, 107019.
57. Adel, A.; El-Shafei, A.; Ibrahim, A.; Al-Shemy, M.; Extraction of Oxidized Nanocellulose from Date Palm (*Phoenix Dactylifera* L.) Sheath Fibers: Influence of CI and CII Polymorphs on the Properties of Chitosan/Bionanocomposite Films. *Ind. Crop. Prod.* **2018**, *124*, 155–165.
58. Mehanny, S.; Abu-El Magd, E.E.; Ibrahim, M.; Farag, M.; Gil-San-Millan, R.; Navarro, J.; El Habbak, A.E.H.; El-Kashif, E; Extraction and Characterization of Nanocellulose from Three Types of Palm Residues. *J. Mater. Res. Technol.* **2021**, *10*, 526–537.
59. Jiang, Q.; Zhang, H.; Yang, J.; Wu, L.; Zhang, H. Nanobubbles Create Hierarchical Pores of Cryogels Based on Chitosan and Regenerated Silk Fibroin: Accelerating Oil Absorption in Constructing Foam-Templated Oleogels. *Food Hydrocoll.* **20205**, *166*, 111312.
60. Srisuwan, Y.; Baimark, Y.; Srihanam, P. Preparation of Regenerated Silk Sericin/Silk Fibroin blend Microparticles by Emulsification-Diffusion Method for Controlled Release Drug Delivery. *Particul. Sci. Technol.* **2017**, *35*, 387–392.
61. Wongnarat, C.; Srihanam, P. Biomaterial Microparticles of Keratose/Collagen blend Prepared by a Water-in-Oil Emulsification-Diffusion Method. *Particul. Sci. Technol*. **2020**, *31*, 379–384.

 doi:10.20944/preprints202605.0850.v1

62. Imsombut, T.; Srisa-ard, M.; Srihanam, P.; Baimark, Y.; Preparation of Silk Fibroin Microspheres by Emulsification-Diffusion Method for Controlled Release Drug Delivery Applications. *E-Polymers* **2011**, *88*, 1-8.
63. Karatzos, S.K.; Edye, L.A.; Orlando, W.; Doherty, S.; Sugarcane Bagasse Pretreatment Using Three Imidazolium - based Ionic Liquids: Mass Balances and Enzyme Kinetics. *Biotechnol. Biofuels* **2012**, *5*, 1-12.
64. Li, B.; Sun, Y.; Yao, J.; Wu, H.; Shen, Y.; Zhi, C.; Li, J. An Environment-Friendly Chemical Modification Method for Thiol Groups on Polypeptide Macromolecules to Improve the Performance of Regenerated Keratin Materials. *Mater. Des.* **2022**, *217*, 110611.
65. Pakkaner, E.; Yalçın, D.; Uysal, B.; Top, A.; Self - Assembly Behavior of the Keratose Proteins Extracted from Oxidized *Ovis aries* Wool Fibers. *Int. J. Biol. Macromol*. **2019**, *125*, 1008-1015.
66. Liu, Q.; Ying, G.; Jiang, N.; Yetisen, A.K.; Yao, D.; Xie, X.; Fan, Y.; Liu, H.; Three-Dimensional Silk Fibroin Microsphere-Nanofiber Scaffolds for Vascular Tissue Engineering. *Med. Nov. Technol. Devices* **2021**, *9*, 100051.
67. Pakkaner, E.; Yalçın, D.; Uysal, B.; Top, A. Self - Assembly Behavior of the Keratose Proteins Extracted from Oxidized *Ovis aries* Wool Fibers. *Int. J. Biol. Macromol.* **2019**, *125*, 1008-1015.
68. Sharma, S.; Gupta, A.; Chik, S.M.S.T.; Kee, C.G.; Mistry, B.M.; Kim, D.H.; Sharma, G. Characterization of Keratin Microparticles from Feather Biomass with Potent Antioxidant and Anticancer Activities. *Int. J. Biol. Macromol.* **2017**, *104*, 189-196.
69. Melo-Silveira, R.F.; Fidelis, G.P.; Costa, M.S.S.P.; Telles, C.B.S.; Dantas-Santos, N.; Elias, S.O.; Ribeiro, V.B.; Barth, A.L.; Macedo, A.J.; Leite, E.L.; Rocha, H.A.O. In Vitro Antioxidant, Anticoagulant and Antimicrobial Activity and in Inhibition of Cancer Cell Proliferation by Xylan Extracted from Corn Cobs. *Int. J. Mol. Sci.* **2012**, *13*, 409–426.
70. Wolkers, W.F.; Oliver, A.E.; Tablina, F.; Crowea, J.H. A Fourier-Transform Infrared Spectroscopy Study of Sugar Glasses. *Carbohydr. Res.* **2004**, *339*, 1077–1085.
71. Silva, F.R.F.; Dore, C.M.P.G.; Marques, C.T.; Nascimento, M.S.; Benevides, N.M.B.; Rocha, H.A.O.; Chavante, S.F.; Leite, E.L. Anticoagulant Activity, Paw Edema and Pleurisy Induced Carrageenan: Action of Major Types of Commercial Carrageenans. *Carbohydr. Polym.* **2010**, *79*, 26–33.
72. Lim, S.H.; Hudson, S.M. Synthesis and Antimicrobial Activity of a Water-Soluble Chitosan Derivative with a Fiber-Reactive Group. *Carbohydr. Res.* **2004**, *339*, 313–319.
73. Biswas, S.; Rahaman, T.; Gupta, P.; Mitra, R.; Dutta, S.; Kharlyngdoh, E.; Guha, S.; Ganguly, J.; Pal, A.; Das, M.; Cellulose and Lignin Profiling in Seven, Economically Important Bamboo Species of India by Anatomical, Biochemical, FTIR Spectroscopy and Thermogravimetric Analysis. *Biomass Bioenerg*. **2022**, *158*, 106362.
74. Vino, A.B.; Ramasamy, P.; Shanmugam, V.; Shanmugam, A. Extraction, Characterization and Iin Vitro Antioxidative Potential of Chitosan and Sulfated Chitosan from Cuttlebone of Sepia aculeata Orbigny, 1848. *Asian. Pac. J. Trop. Biomed.* **2012**, *2*, S334–S341.
75. Song, C.; Yu, H.; Zhang, M.; Yang, Y.; Zhang, G. Physicochemical Properties and Antioxidant Activity of Chitosan from the Blowfly *Chrysomya megacephala* Larvae. *Int. J. Biol. Macromol.* **2013**, *60*, 347–354.
76. Wang, T.; Zhao, Y. Optimization of Bleaching Process for Cellulose Extraction from Apple and Kale Pomace and Evaluation of their Potentials as Film Forming Materials. *Carbohydr. Polym.* **2021**, *253*, 117225.
77. Du, H.; Liu, W.; Zhang, M.; Si, C.; Zhang, X.; Li, B. Cellulose Nanocrystals and Cellulose Nanofibrils Based Hydrogels for Biomedical Applications. *Carbohydr. Polym.* **2019**, *209*, 130-144.
78. Khan, A.; Khan, R.A.; Salmieri, S.; Le Tien, C.; Riedl, B.; Bouchard, J.; Chauve, G.; Tan, V.; Kamal, M.R.; Lacroix, M. Mechanical and Barrier Properties of Nanocrystalline Cellulose Reinforced Chitosan Based Nanocomposite Films. *Carbohydr. Polym.* **2012**, *90*, 1601–1608.
79. Rojas-Lema, S.; Nilsson, K.; Trifol, J.; Langton, M.; Gomez-Caturla, J.; Balart, R.; Garcia-Garcia, D.; Morina, R.; Faba Bean Protein Films Reinforced with Cellulose Nanocrystals as Edible Food Packaging Material. *Food Hydrocoll.* **2021**, *121*, 107019.
80. Srihanam, P.; Simchuer, W.; Chounlamany, V.; Phomkeona, K.; Deevanhxay, P.; Baimark, Y. Reinforcement of Thermo-Compressed Sodium Alginate Films with Calcium Alginate Powder. *Mar. Drugs* **2026**, *24*, 142.

 doi:10.20944/preprints202605.0850.v1

81. Kaur, P.; Choudhary, A.; Thakur, R. Synthesis of Chitosan-Silver Nanocomposites and their Antibacterial Activity. *Int. J. Sci. Eng. Res.* **2013**, *4(4)*, 869–872.
82. Morsy, M.; Mostafa, K.M.; Amyn, H.A.-M.; El-Ebissy, A.A.h.; Salah, A.M.; Youssef, M.A. Synthesis and Characterization of Freeze Dryer Chitosan Nanoparticles as Multifunctional Eco-friendly Finish for Fabricating Easy Care and Antibacterial Cotton Textiles. *Egypt. J. Chem.* **2019**, *62,(7)*, 1277–1293.